applied sciences

MDPI

Article

Investigation of the Fatigue Behaviour of a Ballastless Slab Track–Bridge Structural System under Train Load

Lingyu Zhou, Linqi Yang, Zhi Shan *, Xiusheng Peng and Akim D. Mahunon

School of Civil Engineering & National Engineering Laboratory for High Speed Railway Construction & Engineering Technology Research Center for Prefabricated Construction Industrialization of Hunan Province, Central South University, 68 South Shaoshan Road, Changsha 410075, China

* Correspondence: zhishan@csu.edu.cn; Tel.: +86-0731-82656611

Received: 25 July 2019; Accepted: 23 August 2019; Published: 3 September 2019

Abstract: To probe into the time-dependent behaviour of the ballastless track–bridge structural system under train load, based on the import of the static and fatigue damage constitutive model of materials to simulate damage deterioration of the structural system and interface cohesive zone model to the interface layer, a three-dimensional nonlinear finite element model of the China Railway Track System Type II (CRTS II) ballastless track–bridge structural system was established using the equivalent static method. Then, using this model, we developed the numerical simulation analysis of the influence law of material damage deterioration on structural system performance under train load and revealed the fatigue evolution of the structural system. The results show that the beam remains in compressed status for the whole process, the track is in compression in the midspan and in tension at the beam end, and the tensile stress is larger near the shear groove under the double-track static load. Under the fatigue load, stiffness degradation of the structural system is not obvious, and integral rigidity of the structural system is dependent on the rigidity of the beam. Strength reduction of the materials caused stress redistribution of the structural system and had a larger effect on the stress of each layer of track structure than on the stress on the beam. The fatigue degradation of the cement-emulsified asphalt (CA) mortar layer material has a significant impact on the structural system, which directly affects structural layer stress variation with the fatigue loading cycle.

Keywords: ballastless track–bridge structural system; constitutive model; fatigue damage; finite element analysis; fatigue performance; cement-emulsified asphalt mortar

1. Introduction

The China Railway Track System Type II (CRTS II) ballastless slab track is widely used in China's national high-speed railway system due to its various advantages such as running comfort and high structural stability [1,2]. As the ballastless track–bridge structural system composed of CRTS II slab track is a vertical multilayer spatial structure, the randomness and time-dependent material properties of structural layers, the interlayer connection nonlinearity and the boundary condition complexity are a series of factors that inevitably impact the mechanical fatigue properties of the structural system under train load, thus affecting the running comfort and safety of the high-speed trains and increasing the difficulty of maintenance.

The existing literature mainly focuses on investigating the fatigue properties of the track system concrete structure [3–8], the fatigue properties of the cement-emulsified asphalt (CA) mortar material [9–14], and the interlayer connection between the concrete and CA mortar [15–20]. They consider neither the fatigue damage of CA mortar layer, the influence of the beam on the track system

nor the impact of the track system interface damage on the mechanical properties of the structural system. For example, based on the deterministic static and fatigue constitutive law of concrete materials, Wang Qing et al. [4] established the fatigue finite element model of the CRTS II ballastless slab track. The study shows that the stress and displacement of the track structure tend to be stable after 20 years under the coupled action of temperature and repeated train loads. Poveda [5] studied the fatigue life of the ballastless slab track structure in Japan through the full-scale test and numerical analysis. The results show that the strength of the slab concrete should not be less than 50 MPa to ensure a track structure of 100 years of fatigue life. Additionally, to minimize the track structure fatigue damage, the slab thickness should not be less than 0.17 m. Liu [9] studied the effects of different temperature gradients and Combined loads on the mechanical properties of the CRTS II ballastless slab track. The study concluded that the temperature gradient was one of the main factors leading to the gap between the slab layer and the CA mortar layer that would further accelerate the degradation of the slab and the CA mortar layer. Du [10] used the Palmgren–Miner linear fatigue cumulative damage criterion to analyse and predict the fatigue life of CA mortar layer under different train loads. The results show that the CA mortar layer fatigue life decreases with the increase in train loads, and the position of CA mortar layer that experiences the most unfavourable fatigue life is at the end of the track. Zhu [14] used the cohesive zone model for an interface to establish the vehicle-track coupling model, analysed the damage fracture and delamination between the slab layer and the CA mortar layer under the coupled action of temperature and train load. The results show that the lateral warping of the slab caused by cooling leads to severe interface damage on both sides of the track, while the longitudinal interface damage is not apparent. The interface damage has a significant influence on the dynamic response of the track structure. Zhong Yanglong [15] introduced the cohesive zone law for the interface to simulate the interlayer interaction between the slab layer and the CA mortar layer. The study also established the finite element model of CRTS II slab track interlayer shear failure to analyse the track interlayer shear failure law under temperature, and found that the increase of interlayer shear strength and fracture toughness could control the occurrence of interlayer cracks and enhance the longitudinal stability of the track. At the same time, Xu Qingyuan et al. [21–23] carried out mechanical tests and numerical simulation on fatigue characteristics of a ballastless track supported by a bridge and achieved a series of results.

Based on the existing research results on static and the fatigue constitutive law of concrete and CA mortar layer [24–26] and introducing a cohesive zone model, this paper establishes a three-dimensional finite element model of the CRTS II ballastless slab track–bridge structural system and uses an equivalent static method to analyse the mechanical fatigue properties of the structural system under double-track train load.

2. Material Constitutive Model and Interface Cohesive Zone Model

2.1. Static and Fatigue Damage Constitutive Model of Concrete

Among a number of damage models [25,27], a fibre bundle–plastic chain model (BCM) [25] is developed based on the classical fibre bundle model (FBM) for characterising the mechanical behaviours of quasi-brittle materials under external loading. The damage model BCM was verified to be able to capture the stochastic microstructure and the crack/damage behaviours of concrete material and describe the stress–strain curve under fatigue loading precisely and conveniently [25]. According to the constitutive law recommended in the concrete structure design specification [27], the concrete static constitutive model can be determined by the regression method [25]:

$$\sigma^{\pm} = (1 - d^{\pm}) E_0 \varepsilon^{\pm} \quad (1)$$

The damage evolution law of tensile concrete is as follows.

$$d^+ = A_1^+ + \left(A_2^+ - A_1^+\right)\left[\frac{c}{1+10^{p_1\cdot(x_1-x)}} + \frac{1-c}{1+10^{p_2\cdot(x_2-x)}}\right] \tag{2}$$

The damage evolution law of compressive concrete is as follows.

$$d^- = \frac{A_1^- - A_2^-}{1+(x/x_0)^{p_3}} + A_2^- \tag{3}$$

$$x = \frac{\varepsilon}{\varepsilon_{\mathrm{k}}^{\pm}} \tag{4}$$

where $\sigma^{\pm}$ and $\varepsilon^{\pm}$ denote the concrete tensile (compressive) stress and strain, respectively; E_0 is the initial elastic modulus of concrete; $A_1{}^+$, $A_2{}^+$, c, p_1, p_2, x_1, and x_2 are parameters related to the tensile damage of concrete material and can be obtained from the literature by the authors [25]; $A_1{}^-$, $A_2{}^-$, p_3, and x_0 are parameters related to the compressive damage of concrete material that can be obtained from the literature by the authors [25]; and $\varepsilon^{\pm}{}_{\mathrm{k}}$ is the uniaxial tensile (compressive) strain corresponding to the peak strain of the concrete.

Furthermore, the fatigue degradation of concrete under cyclic loading is characterised by elastic deformation damage and irreversible deformation damage [25]. Considering the time-dependent and random patterns of the concrete material damage, the concrete fatigue constitutive law is established by the regression method [25]:

$$\sigma_n^{\pm} = (1-d_n^{\pm})E_0\varepsilon_n^{\pm} \tag{5}$$

The concrete fatigue damage variable evolution law is

$$d_n^{\pm} = d_1^{\pm} + d_0^{\pm}\cdot\left(d_N^{\pm} - d_1^{\pm}\right) \tag{6}$$

where the normalised damage variable is

$$d_0^{\pm} = A_3^{\pm}\left(-\frac{n/N}{n/N - A_4^{\pm}}\right)^{\frac{1}{A_5^{\pm}}} \tag{7}$$

For compressive concrete, the irreversible deformation damage variable is

$$d_{\mathrm{i},n}^- = \begin{cases} d_n^-, & d_n^- \le 0.2 \\ \frac{1}{-5d_n^-+6}, & d_n^- > 0.2 \end{cases} \tag{8}$$

while the irreversible deformation damage variable of tensile concrete is

$$d_{\mathrm{i},n}^+ = \frac{d_n^+ - d_{\mathrm{e},n}^+}{1-d_{\mathrm{e},n}^+} \tag{9}$$

where the fatigue elastic deformation damage variable is

$$d_{\mathrm{e},n}^+ = \begin{cases} 0, & \varepsilon^+ \le 115.5\times10^{-6} \\ 1-\left(\frac{\varepsilon^+}{115.5\times10^{-6}}\right)^{-1.05}, & \varepsilon^+ > 115.5\times10^{-6} \end{cases} \tag{10}$$

The fatigue life can be calculated by the following formula [28].

$$\log N^{\pm} = 14.7 - 13.5\frac{\sigma_{\max}^{\pm} - \sigma_{\min}^{\pm}}{f_k^{\pm} - \sigma_{\min}^{\pm}} \tag{11}$$

where n is the number of loading cycles for a given stress range; N is the fatigue life (number of loading cycles that causes fatigue failure); ${\sigma^{\pm}}_n$ and ${\varepsilon^{\pm}}_n$ are the concrete tensile (compressive) stress and strain after the nth fatigue loading cycle, respectively; ${d^{\pm}}_1$ and ${d^{\pm}}_N$ denote the concrete tensile (compressive) damage variables under the first and the Nth fatigue loading cycle, respectively; the parameters ${A_3}^{\pm}$, ${A_4}^{\pm}$, and ${A_5}^{\pm}$ can be determined through experimental test to draw the normalised damage variable ${d^{\pm}}_0$; ${\sigma^{\pm}}_{\max}$ and ${\sigma^{\pm}}_{\min}$ are the maximum and minimum fatigue stress, respectively; and ${f_k}^{\pm}$ represents the tensile (compressive) strength of the concrete.

2.2. Static and Fatigue Damage Constitutive Model of the CA Mortar

The CA mortar filling layer is a key component of the CRTS II high-speed railway ballastless slab track structure in China. It not only bears the vertical load but also restricts the horizontal movement of the slab and enhances the integrity of the track structure. However, the existing literature rarely reports the constitutive law of this layer material. In this paper, the static and fatigue viscoelastic-damage constitutive model of the CA mortar as determined in the final test report [26] is introduced in order to study the effect of fatigue degradation of CA mortar layer on the mechanical properties of the ballastless track–bridge structural system. Based on the BCM for concrete material [25], the static and fatigue viscoelastic-damage constitutive model (i.e., a fibre bundle–plastic chain model for CA mortar material) [26] was developed for characterising the mechanical behaviours of the material under external loading. The viscoelastic-damage model for CA mortar was verified to be able to capture the stochastic microstructure and the viscoelastic-damage behaviours of CA mortar material and describe the stress–strain curve under fatigue loading precisely and conveniently [26]. It considered the both the effects of microviscoelastic-damage behaviours due to micro asphalt gel and the fatigue failure due to external loading [26]. The predicted fatigue life of the CA mortar agrees with the experimental results [26].

The following Equation (12) presents the compression stress–strain law of the CA mortar material of the CRTS II slab track obtained by the uniaxial compression test [26].

$$\sigma = 1.761 \times 10^{-7} \varepsilon^{6.069\varepsilon^{-0.137}} \tag{12}$$

Since the current literature [26] does not report a tensile test of the CA mortar material of the CRTS II slab track, for simplicity, the stress of the static and fatigue damage constitutive law for the CRTS II CA mortar material slab track under tension are taken as 1/10 of the tress of the static and fatigue damage constitutive law under compression corresponding to certain strain [27]. The following is only a brief description of the fatigue damage constitutive model of CA mortar material under compression;

$$\sigma = (1 - D_{\mathrm{M}}) E_{\mathrm{f0}} \varepsilon \tag{13}$$

with the fatigue damage variable under the nth fatigue loading cycle presented below.

$$D_{\mathrm{M}}(n/N) = A_{\mathrm{M},3} \cdot \left(-\frac{n/N}{n/N - A_{\mathrm{M},4}} \right)^{\frac{1}{A_{\mathrm{M},5}}} \tag{14}$$

The irreversible deformation fatigue damage variable under the nth fatigue loading cycle can be calculated with the following Equation (15).

$$D_{\mathrm{M,i}}(n/N) = \frac{1}{7.694 - 3.342 \times \left[1 - e^{-\frac{D_{\mathrm{M}}(n/N)}{0.343}} \right] - 2.375 \times \left[1 - e^{-\frac{D_{\mathrm{M}}(n/N)}{0.0113}} \right]} \tag{15}$$

where $A_{\mathrm{M},3}$, $A_{\mathrm{M},4}$ and $A_{\mathrm{M},5}$ are parameters related to the fatigue damage characteristics of the CA mortar. Their values can be determined by the test results data fitting method.

The fatigue (dynamic) elastic modulus under the nth fatigue loading cycle can be expressed as

$$E_{\mathrm{M}fn} = \frac{\Delta\varepsilon_1}{\Delta\varepsilon_n} E_{\mathrm{M}f0} \tag{16}$$

$$\Delta\varepsilon_1 = \varepsilon_{\max,1} - \varepsilon_{\mathrm{i},1} \tag{17}$$

$$\Delta\varepsilon_n = \varepsilon_{\max,n} - \varepsilon_{\mathrm{i},n} \tag{18}$$

Total strain under the first fatigue loading cycle is

$$\varepsilon_{\max,1} = 286.3 + 1315.5S \tag{19}$$

Total strain under the Nth fatigue loading cycle (when Fatigue Failure occurred) is

$$\varepsilon_{\max,N} = 1177.4 + 3023.1S \tag{20}$$

Total strain under the nth fatigue loading cycle is

$$\varepsilon_{\max,n} = \varepsilon_{\max,1} + D_{\mathrm{M}}(n/N) \cdot (\varepsilon_{\max,N} - \varepsilon_{\max,1}) \tag{21}$$

The residual strain under the nth fatigue loading cycle is

$$\varepsilon_{\mathrm{i},n} = D_{\mathrm{M,i}}(n/N) \cdot \varepsilon_{\max,n} \tag{22}$$

Fatigue life calculation as shown in Equation (23):

$$\lg N = 10.075 - 8.045S \tag{23}$$

where S is the stress level, which is the ratio of the maximum compressive (tensile) stress to the compressive (tensile) strength.

2.3. Interface Cohesive Zone Constitutive Model

The cohesive zone model, which is widely used in interface damage and cracking of composite materials analysis, can accurately estimate the crack initiation and propagation process on the cracking path and can better describe the nonlinear interlayer damage behaviour of concrete [29]. The cohesive zone theory is characterised by the interface constitutive law, which is the relationship between interface adhesion and interface displacement and cracking. The standard cohesive zone constitutive models are bilinear, exponential, trapezoidal and plastic cohesive zone models. For the problem of interlayer bond damage of track structures, the bilinear cohesive zone model is adopted in the literature [30], as shown in Figure 1.

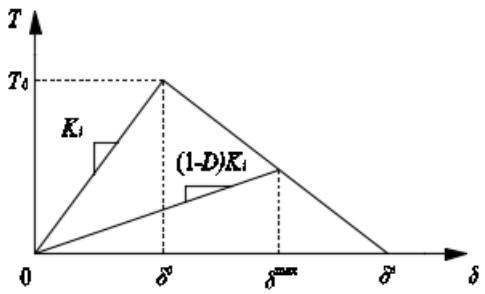

Figure 1. Bilinear cohesive zone model.

The model assumes that the interface stiffness *K*i (including normal and tangential stiffness) decreases linearly dependent on the interface displacement after the damage increases. The formula of damage variable D is given by the following Equation (24).

$$D = \begin{cases} 0, & 0 \le \delta^{\max} \le \delta^0 \\ \frac{\delta^c\left(\delta^{\max}-\delta^0\right)}{\delta^{\max}\left(\delta^c-\delta^0\right)}, & \delta^0 < \delta^{\max} < \delta^c \\ 1, & \delta^{\max} > \delta^c \end{cases} \tag{24}$$

where δ^0 is the displacement at the time of interlayer interface damage initiation, δ^c is the displacement at the time of interlayer interface crack initiation and $\delta^{\max}$ is the maximum reached displacement during the loading process.

The quadratic nominal stress damage criterion is used to identify the initiation of interface damage. Damage initiation corresponds to the moment at which the sum of the squares of nominal stress ratios in all directions is equal to 1:

$$\left\{\frac{\langle t_n \rangle}{t_n^0}\right\}^2 + \left\{\frac{t_s}{t_s^0}\right\}^2 + \left\{\frac{t_t}{t_t^0}\right\}^2 = 1 \tag{25}$$

where ${t_n}^0$ is the normal strength, and ${t_s}^0$ and ${t_t}^0$ denote the strength in the two tangential directions.

3. Finite Element Model of Ballastless Track–Bridge Structural System

3.1. Parameter Selection

To simulate the track–bridge structural system, the finite element software ANSYS (ANSYS, Inc., Southpointe, 2600 ANSYS Drive, Canonsburg, PA 15317, USA) was used to establish a nonlinear three-dimensional finite element model of a 3-span (a span of 32 m for each) CRTS II ballastless slab track-simple supported bridge structure (Figure 2). See "Post-tensioned Prestressed Concrete Simply Supported Box Girder of Prefabricated Ballastless Track for 350 km/h High-Speed Railway" Standard drawings for the number and shape arrangement of beams. The ANSYS Solid65 element and the Link8 element were used to model the bridge and the prestressing strands, respectively. Figure 3 shows the schematic diagram of the cross-section.

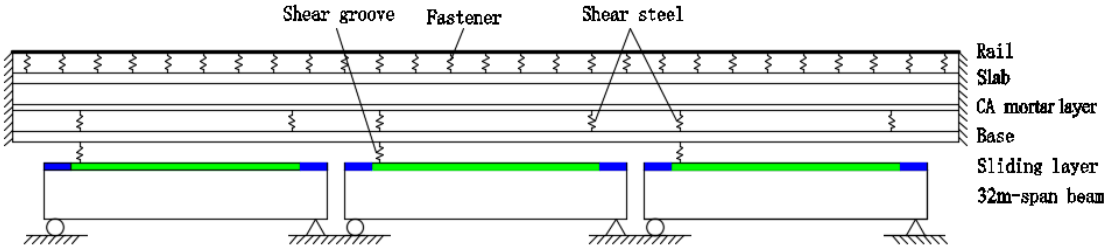

Figure 2. Mechanical model of the ballastless track–bridge structure.

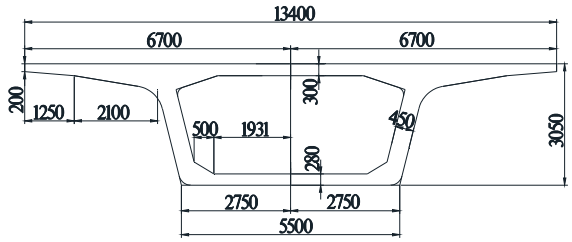

Figure 3. Box beam cross-section (mm).

The track structure is composed of slab, CA mortar layer and concrete road-bed (base). To model each component of the track system, ANSYS Solid65 element was also used. The mechanical parameters

of each layer of materials are detailed in Table 1. The heavy rail type CHN60 was modelled by 3D Beam189 element.

Table 1. Mechanical parameters of the track structure.

Structural Parts	Density (kN/m^3)	Thickness (mm)	Poisson Ratio (μ)
Base (C30)	26.00	190	0.2
CA mortar layer	18.00	30	0.2
Slab (C55)	26.00	200	0.2

The values of the parameters in the static constitutive model of concrete material are shown in Tables 2 and 3; the values of the parameters in the fatigue constitutive model are as follows; $A_3{}^+ = 0.701$, $A_4{}^+ = 1.050$, $A_5{}^+ = 8.428$, $A_3{}^- = 0.713$, $A_4{}^- = 1.160$, $A_5{}^- = 5.439$, $A_{M,3} = 0.425$, $A_{M,4} = 1.1$ and $A_{M,5} = 2.7$. The static and the dynamic Young's modulus of CA mortar layer material are $E_{M0} = 5.016$ GPa and $E_{Mf0} = 11.691$ GPa, respectively.

Table 2. Parameters related to the uniaxial tensile constitutive model of the concrete material.

Structural Parts	Base (C30)	Beam (C50)	Slab (C55)
E_t/GPa	25.35	28.75	29.20
A_1+	−0.0897	−0.072	−0.0702
A_2+	1	1	1
x_1	1.20102	1.2005	1.1996
x_2	1.9782	1.8633	1.84728
p_1	2.23984	2.4988	2.54128
p_2	0.56608	0.6325	0.6406
c	0.53486	0.5875	0.5938
ε_k+/10^{-6}	95.24	110.3	112.28

Table 3. Parameters related to the uniaxial compressive constitutive model of concrete material.

Structural Parts	Base (C30)	Beam (C50)	Slab (C55)
E_c/GPa	26.35	31.62	32.51
A_1-	0.00344	0.004036	0.0027
A_2-	1	1	1
x_0	1.06218	1.18968	1.2152
p_3	2.22346	2.88136	3.0432
ε_k-/10^{-6}	1471.8	1678.4	1727

The nonlinear spring Combine39 is used to model fasteners, which are of the WJ-8 type with an ultimate displacement of 2 mm, an unloaded longitudinal peak resistance per rail equal to 24 kN/m, and a loaded longitudinal peak resistance per rail equal to 37.2 kN/m [31]. The track structure interlayer interfaces are simulated by the interface cohesive zone model [30]. The mechanical parameters of the interface between the slab layer and the CA mortar layer are shown in Table 4.

The existing research results show that the shear strength of the interface between C50 concrete and CA mortar layer is lower than the shear strength between C30 concrete and CA mortar layer [32]. Therefore, at the moment of interface damage initiation and interface crack initiation, the displacement at the interface between the base layer and CA mortar layer is taken to be slightly larger than the corresponding displacement at the interface between the CA mortar layer and the slab layer (5 times larger is considered in this paper). Both interfaces are modelled using ANSYS cohesion element Inter205.

Table 4. Parameters related to interface cohesive zone model.

Components	t_0 (MPa)	δ_0 (mm)	δ_c (mm)
Normal direction	1.792	0.0025	0.0282
First tangential direction	0.956	0.0152	0.0376
Second tangential direction	0.956	0.0152	0.0376

The connection mode between the beam and the track structure layers has a significant influence on the overall mechanical performance of the structural system. ANSYS Contact elements CONTA173 and TARGE170 with a friction coefficient equal to 0.2 are used to accurately simulate the "dual textile-one membrane" geotextile sliding interface between the beam and the base.

To connect the slab and the base and coordinate the deformation with each other, shear steel bars are introduced at both ends of the bridge girder joints and the transition section between the side spines and the subgrade. The shear steel bars are simulated by linear spring element Combin14 with longitudinal stiffness of 3.0×10^5 N/mm and vertical tension–compression stiffness of 2.0×10^6 N/mm.

The bridge and the base are provided with shear grooves above the fixed supports to transfer longitudinal forces such as train braking force to the piers. The ANSYS linear spring element Combin14 with a stiffness of 1.0×10^8 N/mm is used to simulate the shear grooves since their connection is nearly rigid.

Based on the abovementioned material constitutive model and interfacial cohesive zone model, as well as the selection of material parameters, geometric dimensions, element types and connection elements of the different parts of the structure, a three-dimensional finite element model of the CRTS II ballastless slab track–simply supported bridge structural system for the high-speed railway is established, as shown in Figure 4.

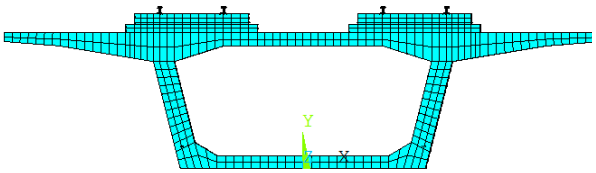

(**a**) Mesh of bridge–track cross-section

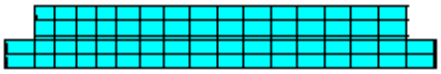

(**b**) Cross-section mesh of track system

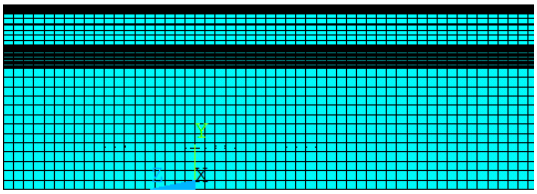

(**c**) Mesh of bridge–track longitudinal -section

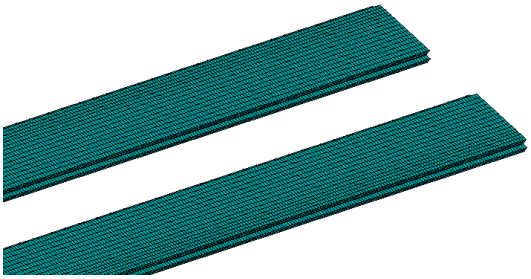

(**d**) Overlooking mesh of track system

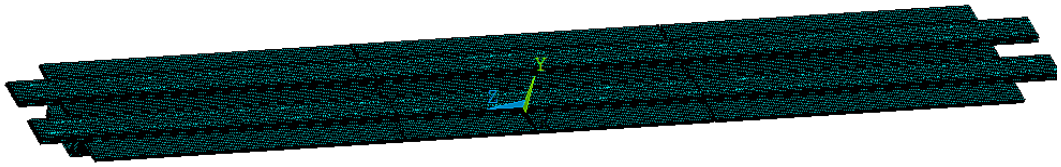

(**e**) Sketch of finite element model of structural system

Figure 4. Finite element model of ballastless track–bridge structure.

3.2. Simplified Calculation Method

The simplified calculation method adopts the equivalent static method [33], which essentially transforms the dynamic fatigue process into a gradual static calculation process. Figure 5 displays a visual representation of the equivalent static analysis process. First, according to the static constitutive model of the abovementioned materials, the stress levels of each structural part under the first fatigue loading cycle are calculated to determine the fatigue life N of the structural layers. Then, the fatigue life cycle ratio n/N is calculated, and the material constitutive law is updated using the fatigue damage model of the abovementioned materials. Finally, the effects of the different fatigue life cycle ratios n/N on the mechanical fatigue properties of the ballastless track–bridge structural system are calculated. According to the three-stage variation law of concrete fatigue performance, the analysis step size should be as small as possible for the first and third stages of fatigue degradation, while for the second stage of stable crack propagation, a larger analysis step size could be selected.

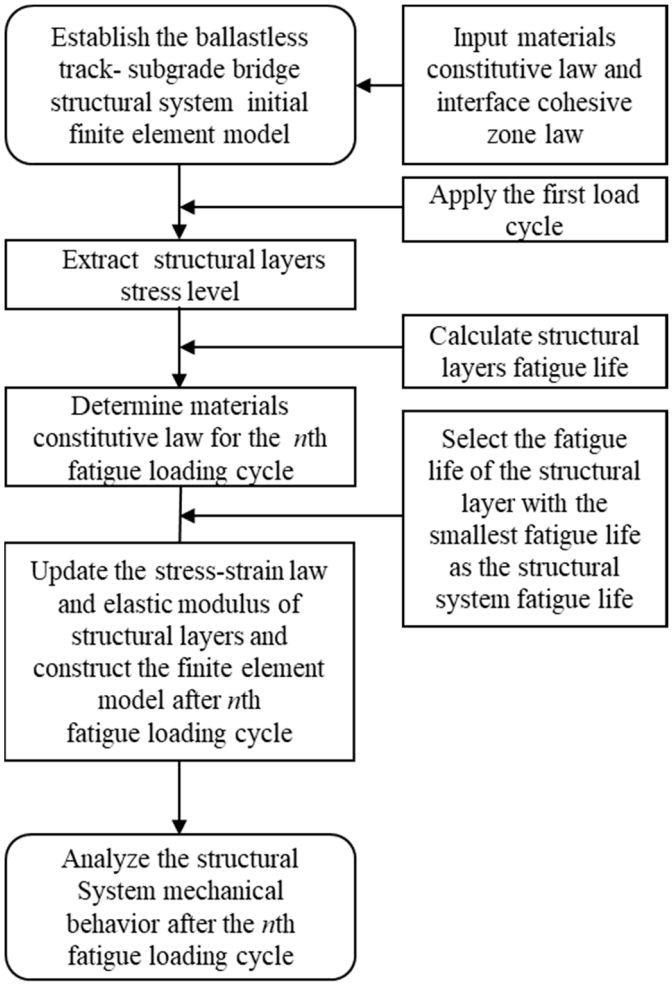

Figure 5. Flow chart of equivalent static analysis for structural system under fatigue loading.

3.3. Verification of Calculation Method

In the work by the authors of [33], ABAQUS software was used to establish a numerical model of a simply supported concrete beam, the predict results were compared to the experimental results in the literature [34], and the validity of the equivalent static analysis method was verified. Considering the issues (such as large test site, expensive test cost and long test time) related to the full-scale test of the ballastless track–bridge structural system under the train fatigue load, a $\frac{1}{4}$-scale indoor model test of a 3-span 32 m CRTS II slab ballastless track–bridge was carried out [35], and the predicted result of

the finite element model was compared to the test results in this paper. The validity of the equivalent static analysis method was further verified.

For the sake of brevity, only the comparison between the test and the finite element model results of the mid-span load–deflection curve of the intermediate beam under static load and that of its top surface reinforcing steel strain under fatigue load is presented in this paper, as shown in Figures 6 and 7. Figure 6 shows that the simulated mid-span load–deflection results of the beam are more significant than the experimental results. However, the maximum error is less than 10%. Figure 7 shows that, although the strain of the beam top surface steel is not apparent with the increase in the fatigue loading cycle, the downward trend is approximately the same, and the error is controlled within 5%. Therefore, this analysis method can be used to analyse the mechanical fatigue properties of the ballastless track–bridge structural system.

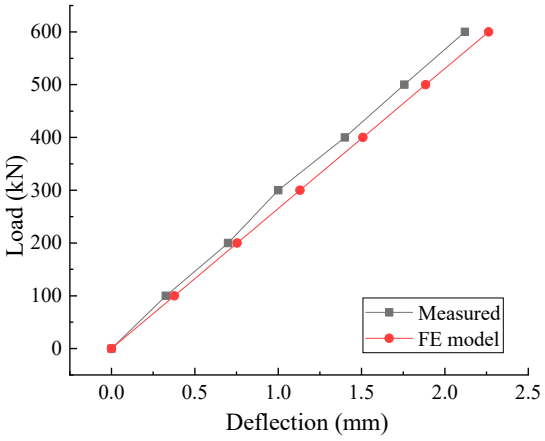

Figure 6. Mid-span load–deflection curve of the beam under static loading.

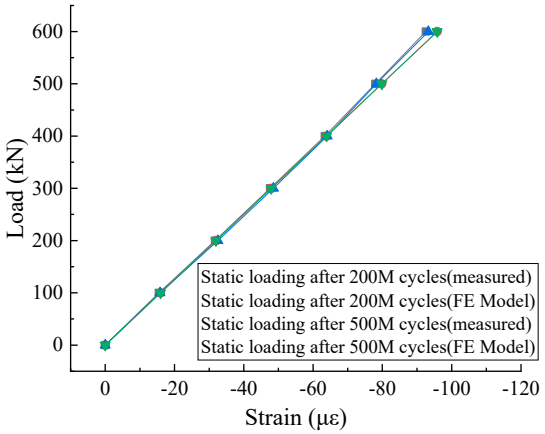

Figure 7. Top surface of beam-reinforcing steel strain under fatigue loading.

4. Numerical Analysis of Mechanical Properties

4.1. Calculation Results Static Mechanical Performance

(1) Static deformation

The deflection curves of the beam and rails under static loads are shown in Figure 8. Since the compressive stress of the track structural layer is low under the action of the vertical train load, the deflection of the layer is consistent with the deflection of the beam, which is not listed here. The maximum deflection of the beam is 6.129 mm while the maximum deflection of the rail is 8.834 mm, and both maximum deflections occur in the mid-span of the intermediate beam, expected since the

vertical train load adopts the China Passenger Transport (ZK) standard live load value [36], which acts on the intermediate beam rail as a larger concentrated load, resulting in more substantial deformation of the spring of the simulated fastener. The relative longitudinal displacement of the beam and the base under static is shown in Figure 9. Due to the "dual textile-one membrane" geotextile sliding layer connection, there is a slip between the beam and the base along the length of the bridge, and the maximum slip occurs at the end of the beam with a magnitude of 1.27 mm.

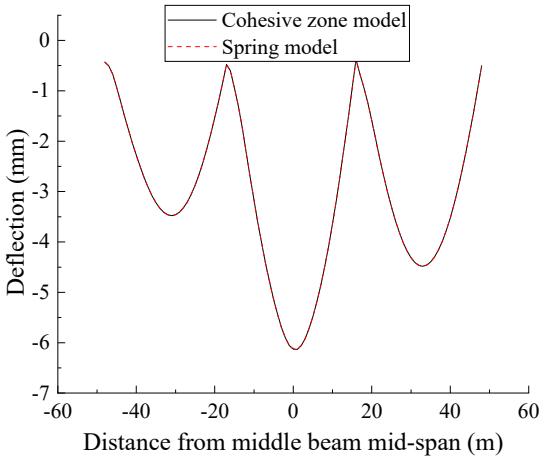

Figure 8. Beam and rail deflection curve under static loading.

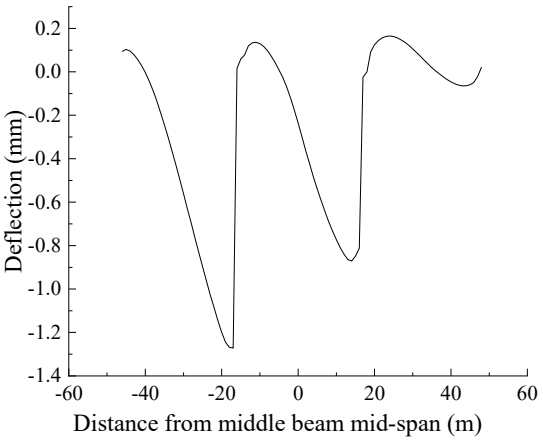

Figure 9. Longitudinal relative displacement of beam and base under static loading.

(2) Static stress

The longitudinal stress distribution of the structural system along the bridge length is shown in Figure 10. The figure shows that the top and the bottom surface of the beam are all in compression under the action of the double-track train load. The longitudinal compressive stress of the simply supported beam top surface gradually decreases from mid-span to the supports, with a maximum magnitude of 4.493 MPa. The longitudinal compressive stress of the beam bottom surface gradually increases from the mid-span to the supports, with a maximum magnitude of 8.147 MPa. Under the action of the double-track train load, all layers of track structure have sudden changes at the beam end because the bridge and track system are connected by a "dual textile-one membrane" geotextile connection layer. Under the action of the train load, the deformation of the bridge and track is inconsistent, and the track system above the beam end is warped and restrained by the bridge. The longitudinal stresses of the top and bottom surface of each layer of the track system substantially coincide with each other in the bridge section. This is not the case for the beam ends where the base bottom surface longitudinal stress is more abrupt than the surface longitudinal stress of its top surface,

and the maximum longitudinal compressive stress at the shear groove near the side beam is 1.535 MPa. The longitudinal stress of the CA mortar layer top and bottom surfaces substantially coincides, and the beam mid-span section longitudinal compressive stress is substantially stable at 0~0.15 MPa. The slab top surface longitudinal stress abruptly changes at the beam end, and the maximum longitudinal tensile stress near the shear groove of the middle beam reaches 2.047 MP. From the stress analysis of the structural system, the fatigue life of the beam can be seen to be controlled by compression, while the fatigue life of the track system layers is controlled by the top surface tensile stress of the layer at the beam end.

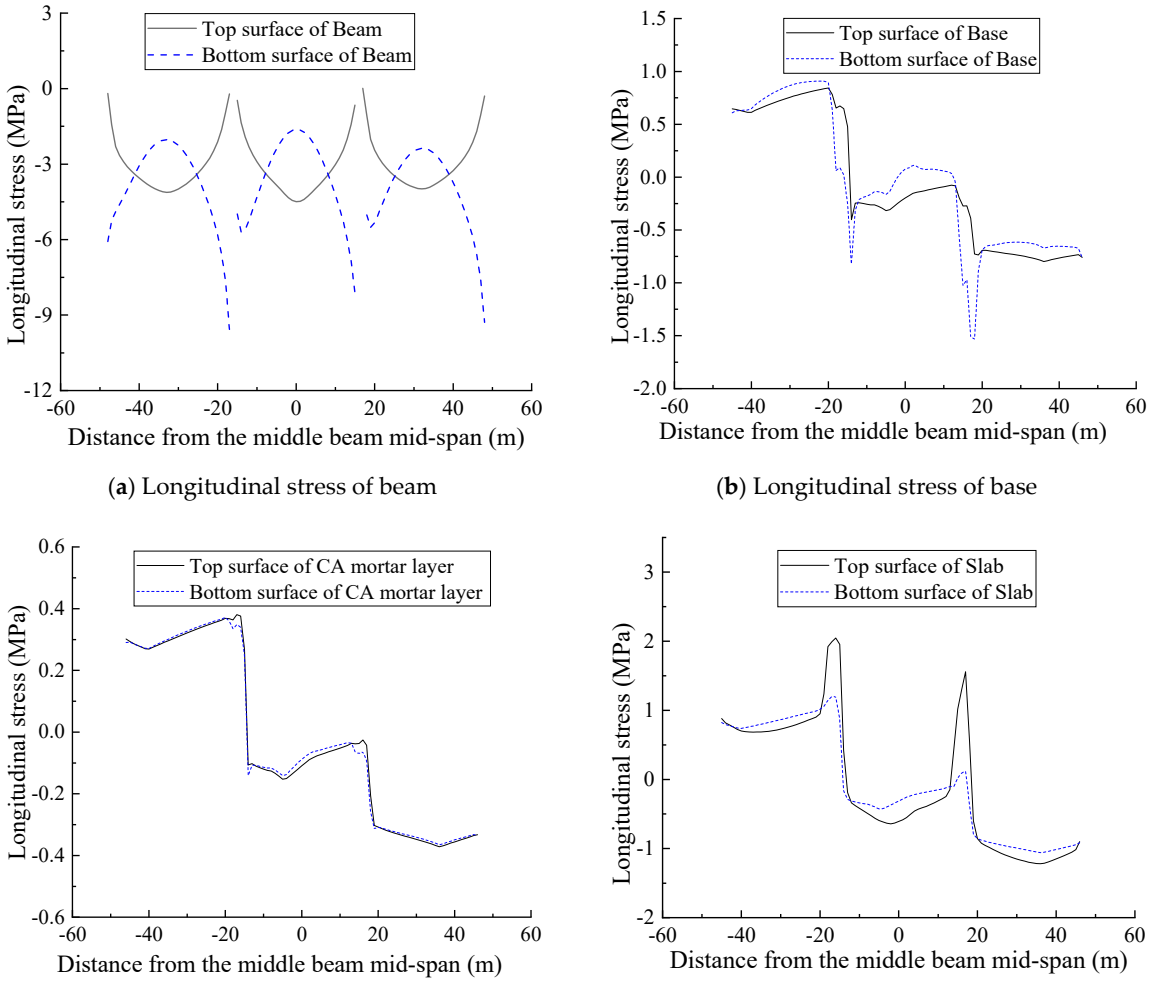

(**a**) Longitudinal stress of beam

(**b**) Longitudinal stress of base

(**c**) Longitudinal stress of CA mortar layer

(**d**) Longitudinal stress of slab

Figure 10. Longitudinal stress of structural layers under static load.

4.2. Fatigue Life Prediction

Based on the finite element model, the fatigue life of the each structural part is calculated using the double-track train load, as shown in Table 5.

Table 5. Fatigue life of structural parts.

Structural Parts	Beam	Base	CA Mortar Layer	Slab
Fatigue life (Cycles)	1.35×10^{12}	2.57×10^{9}	2.98×10^{8}	6.14×10^{8}

Table 5 shows that the fatigue life of the beam under the double-track train load is much longer than the fatigue life of the track system layers, thus the fatigue degradation of the beam can be ignored in the fatigue analysis. The fatigue life of the CA mortar layer is the shortest. Therefore, the fatigue failure of the CA mortar layer can be regarded as the fatigue failure of the track–bridge structural system.

4.3. Analysed Results of Fatigue Performance

(1) Fatigue deformation

The mid-span deflection of the beam under fatigue loading is shown in Figure 11. The figure shows that the deflection at the beam span increases gradually with the number of loading cycles. The increase was significant in the first fatigue stage when the fatigue life ratio is approximately n/N = 10%. Then, the trend shows a steady and slow increase, from 6.129 mm at the initial non-damage stage to 6.383 mm at the failure stage, with a total increase of 4.144%. The stiffness of the structural system evidently degrades gradually with the increase in the fatigue loading cycle, although the degradation is not significant.

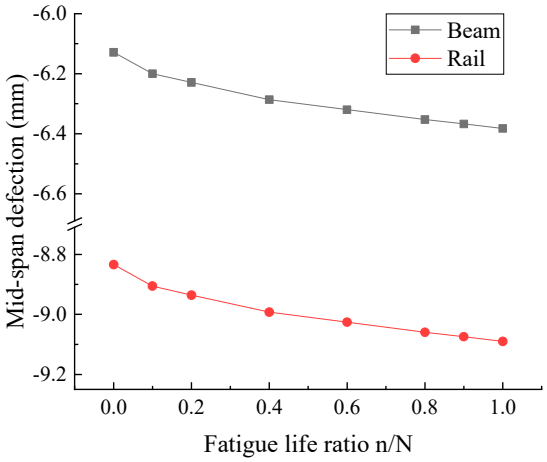

Figure 11. Mid-span deflection response curve of the support beam and the rail under fatigue load.

The rail deflection changes slightly with the increase in the fatigue loading cycle: the initial undamaged rail deflection is 8.834 mm. At the structural system failure stage, the rail deflection increases by 2.898% reaching 9.090 mm. The impact on the track irregularity is minimal, as shown in Figure 12. Figure 13 shows that the mid-span load–deflection of the beam under fatigue load in the numerical simulation is substantially linear, and the change rate is similar to the deflection-fatigue ratio law described in Figure 11: At the initial fatigue loading stage, the slope of the response curve decreases rapidly with the increase in the fatigue loading cycle, and starts to decrease at a steady rate after the fatigue life ratio n/N = 10%, until the structural system fails. The stiffness fatigue degradation of the beam is not apparent. The stiffness fatigue degradation of the track structure has a small effect on the overall stiffness of the structure, since the overall stiffness of the structural system is controlled mainly by the stiffness of the beam.

(2) Fatigue stress

Figure 14 displays the longitudinal stress variation curve for the structural parts under train fatigue load. The figure clearly shows that the mid-span compressive stress of the concrete in the intermediate beam increases slightly with the increase in the fatigue loading cycle, and thus can be neglected. The mid-span longitudinal compressive stress of the CA mortar layer in the intermediate beam decreases in three stages with the increase in the fatigue loading cycle. The difference is that

the top and bottom surfaces longitudinal compressive stress of the slab and that of the base bottom surface's longitudinal tensile stress decrease with the increase of fatigue loading cycle, while the base top surface longitudinal compressive stress increases with the increase in the fatigue loading cycle. The longitudinal stress degradation of structural layers with the fatigue loading cycle is shown in Table 6. The table shows that the layers materials strength degradation leads to stress redistribution in the track–bridge structural system with a significant influence on the layer material stress, although the stress variation of the beam can be neglected.

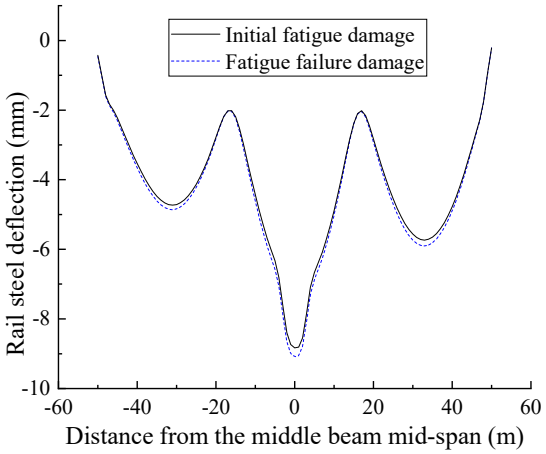

Figure 12. Rail deflection response under static and fatigue load.

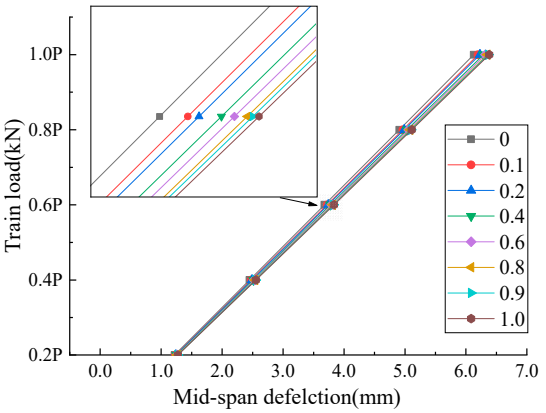

Figure 13. Mid-span load–deflection response curve of the beam under fatigue load.

Table 6. Stress variation in structural parts.

Mid-Span Mid-Section Position	Initial Longitudinal Stress (MPa)	Longitudinal Stress at Failure (MPa)	Variation
Beam top surface	−4.493	-4.497	0.089%
Beam bottom surface	−1.623	−1.625	0.123%
Base top surface	−0.197	−0.20945	6.320%
Base bottom surface	0.07715	0.02364	−69.358%
CA mortar layer top surface	−0.109	−0.088	−19.266%
CA mortar layer bottom surface	−0.080	−0.069	−13.750%
Slab top surface	−0.609	−0.473	−22.332%
Slab bottom surface	−0.312	−0.268	−14.103%

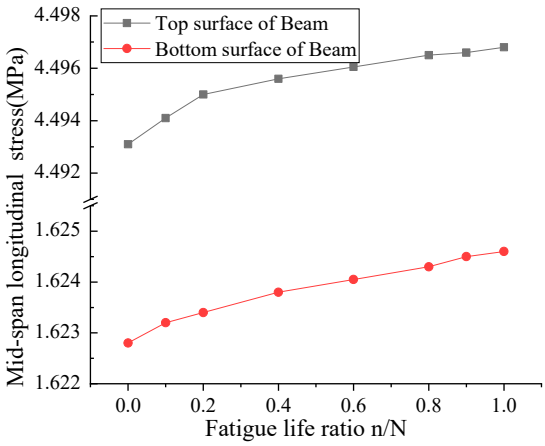

(**a**) Longitudinal stress in intermediate beam concrete

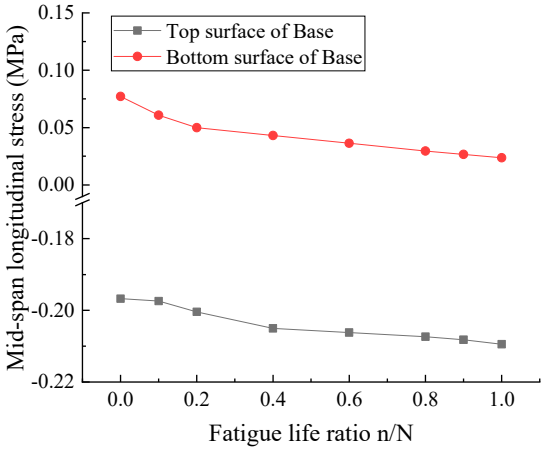

(**b**) Longitudinal stress in base concrete on intermediate beam

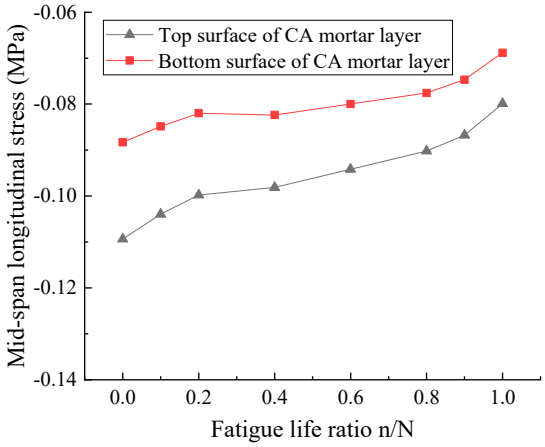

(**c**) Longitudinal stress in cement-emulsified asphalt (CA) mortar layer on intermediate beam

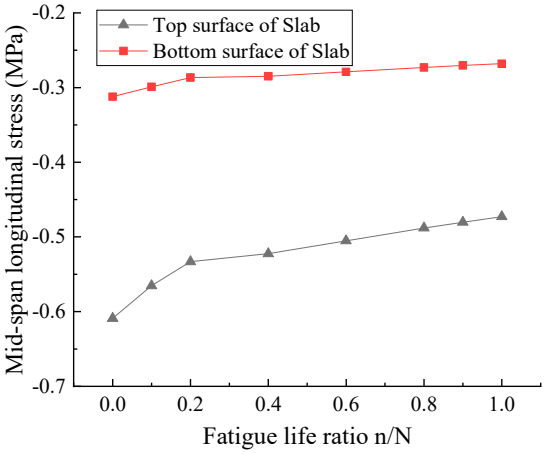

(**d**) Longitudinal stress in slab on intermediate beam

Figure 14. Longitudinal stress on the track–bridge system under fatigue load.

4.4. Effect of Different Interface Bond Simulation Methods on Structural Systems Mechanical Performance

To study the influence of different interface bond simulation methods on the track–bridge system mechanical performance, an interface cohesive zone model and a spring model with the same stiffness were selected for comparison. For brevity reasons, only the comparative analysis of the beam deflection and that of each structural layer top surface are presented in this paper, as shown in Figures 15 and 16. Table 7 shows the maximum calculated values. From Figures 15 and 16 and Table 7, both methods can simulate the interface bond phenomenon because the calculated stress and deformation using interfacial cohesive zone model and spring model with the same stiffness under train loads are almost the same, explained because, under train loads, the track system interlayer bond remains intact when environmental factors, such as temperature and the fatigue damage of the interface, are not considered.

Table 7. Cohesion and spring model comparison.

Interface Bond Models	Beam Maximum Displacement (mm)	Beam Top Surface Maximum Stress (MPa)	Base Top Surface Maximum Stress (MPa)	CA Mortar Layer Top Surface Maximum Stress (MPa)	Slab Top Surface Maximum Stress (MPa)
Cohesive zone model	6.129	−4.493	0.843/−0.797	0.381/−0.372	2.047/−1.218
Spring model	6.133	−4.493	0.841/−0.795	0.379/−0.371	2.026/−1.220

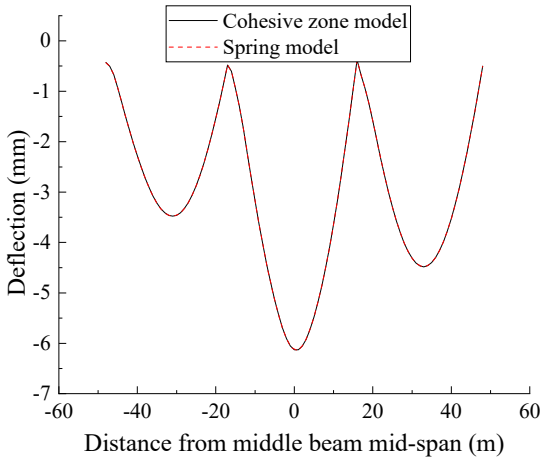

Figure 15. Deflection curves of the beam with the different interfaces bond model under static load.

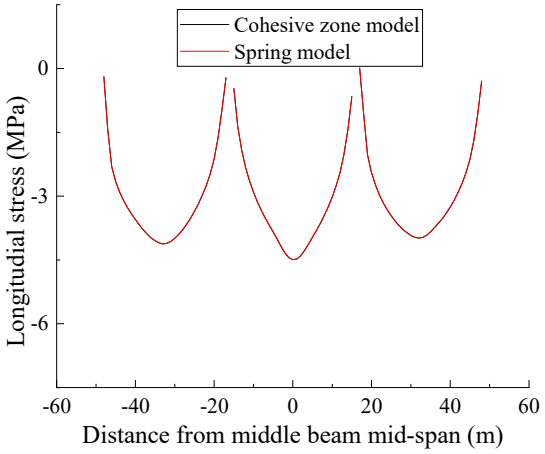

(**a**) Longitudinal stress in the top surface of beam concrete

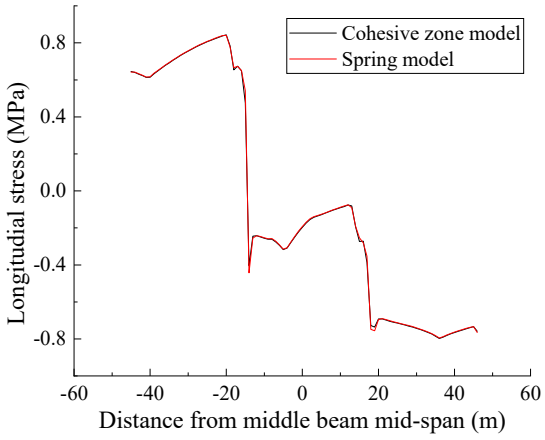

(**b**) Longitudinal stress in in the top surface of base concrete

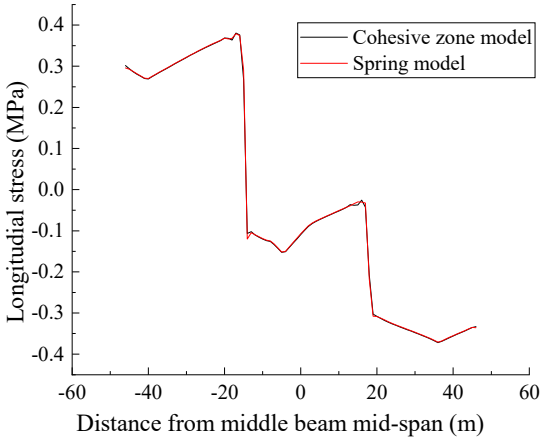

(**c**) Longitudinal stress in the top surface of CA mortar layer

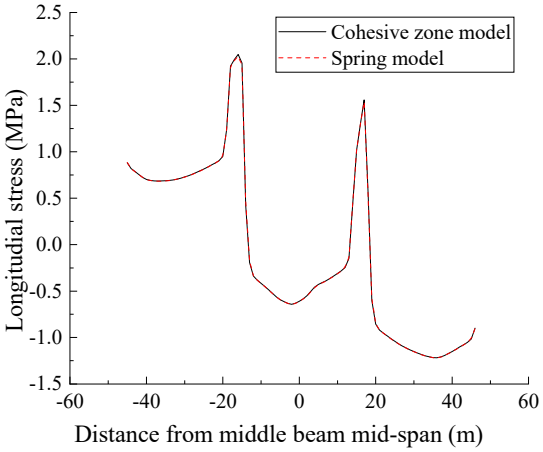

(**d**) Longitudinal stress in the top surface of slab concrete

Figure 16. Longitudinal stress of structural layers with the different interfaces bond model under static load.

4.5. Effect of CA Mortar Layer Fatigue Degradation on Structural System Mechanical Performance

Compared to the existing literature, the main innovation of this paper lies in the introduction of CA mortar static and fatigue damage constitutive law into the structural system simulation. To study the effect of CA mortar layer degradation on the structural system mechanical performance, relevant simulation analysis was carried out. The analysis results are shown in Tables 8 and 9 and Figures 17 and 18. Table 5 shows that, when CA mortar layer damage is not considered, the structural system fatigue life is controlled by the slab and is doubled compared to when the CA mortar layer damage is considered.

Table 8. Summary of beam and rail deflection variation.

Structural Parts	Initial Stage Displacement (mm)	Structural Failure Deflection, Regardless of CA Mortar Layer Damage (mm)	Variation	Structural Failure Deflection, Considering CA Mortar Layer Damage (mm)	Variation
Beam	6.129	6.556	6.967%	6.383	4.144%
Rail	8.834	9.274	4.981%	9.090	2.898%

Table 9. Summary structural parts fatigue degradation considering only the concrete material damage.

Mid-Span Position of the Middle Beam	Initial Longitudinal Stress (MP)a	Failure Longitudinal Stress (MPa)	Variation
Beam top surface	−4.493	−4.501	0.178%
Beam bottom surface	−1.623	−1.625	0.136%
Base top surface	−0.197	−0.241	22.249%
Base bottom surface	0.07715	−0.021	−127.090%
CA mortar layer top surface	−0.109	−0.161	47.817%
CA mortar layer bottom surface	−0.080	−0.140	74.438%
Slab top surface	−0.609	−0.341	−44.085%
Slab bottom surface	−0.312	−0.217	−30.388%

Unlike when CA mortar layer damage is considered, the mid-span deflection of the beam, when only considering concrete materials damage, increases in three stages by 6.967% (from 6.129 mm at the initial non-damaged condition to 6.556 mm at the structural system failure condition), as the loading cycle increases. The rail maximum deflection increases by 4.981% (from 8.834 mm at the initial undamaged condition to 9.274 mm at the slab failure), as shown in Figure 17 and Table 8.

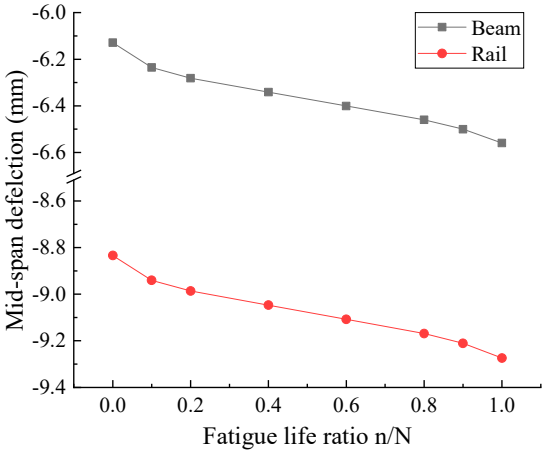

Figure 17. Mid-span deflection curve of beam and rail under fatigue load regardless of CA mortar layer damage.

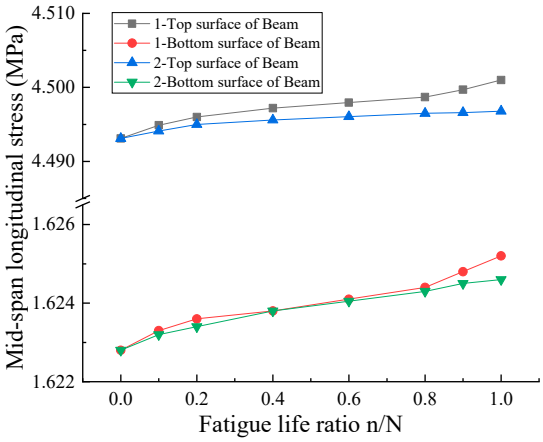

(**a**) Longitudinal stress in intermediate support beam concrete

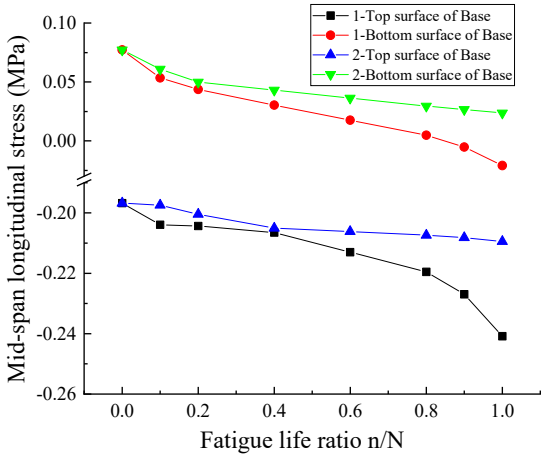

(**b**) Longitudinal stress in intermediate support beam concrete

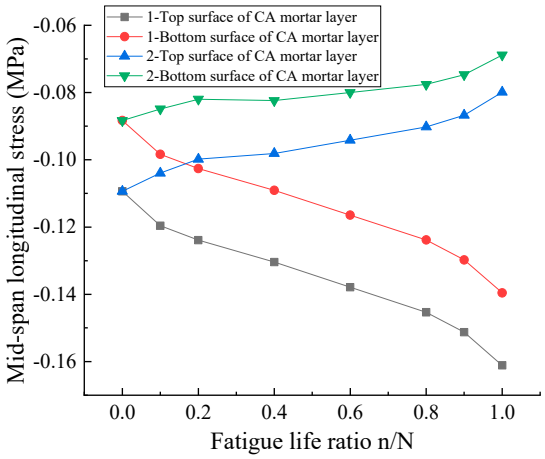

(**c**) Longitudinal stress in intermediate CA mortar layer

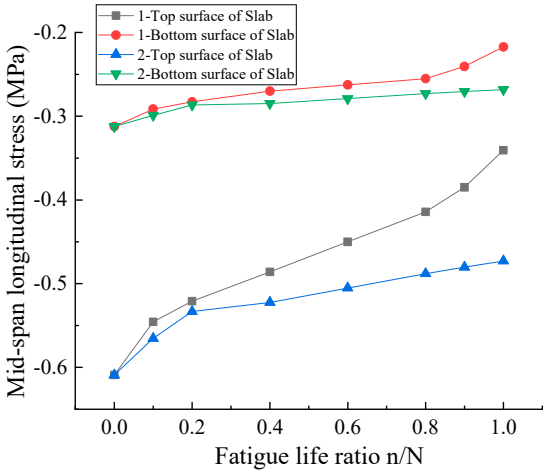

(**d**) Longitudinal stress in intermediate base concrete

Figure 18. Longitudinal stress of structural parts considering or regardless of CA mortar layer degradation. Note: 1: denotes the longitudinal stress regardless of CA mortar layer degradation; 2: denotes the longitudinal stress considering CA mortar layer degradation.

Figure 18 and Table 9 show that the CA mortar layer material fatigue degradation has a high impact on the structural system: under double-track train fatigue load, only the longitudinal stress of the CA mortar layer varies in three stages with fatigue load cycle when CA mortar layer material fatigue degradation is considered. Regardless of CA mortar layer material fatigue degradation, the material of each layer varies in three stages with the fatigue load cycle. The concrete strength degradation also results in stress redistribution of the track–bridge structural system, which has a more significant effect on the track system layer stress than the beam stress. Therefore, the simulation results for the structural system considering the CA mortar layer fatigue degradation are closer to the reality.

5. Conclusions

The following main conclusions can be obtained from the research presented in this paper.

(1) The static, fatigue damage models and the interface cohesive zone model of concrete and CA mortar are introduced. The fatigue lifetime of each structural part is calculated, and the fatigue

failure order is CA mortar layer, slab, base and beam. The fatigue lifetime of the beam is much longer than the fatigue lifetime of the track structure layers.

(2) Under the static train load, as the beam deformation is inconsistent with the deformation of the track system, all the track system layers have an abrupt deformation change at both ends, and their most unfavourable position also occurs at the beam end.

(3) Under the train fatigue load, the stiffness of the structural system experiences a gradual but insignificant degradation. The overall stiffness of the structural system is controlled mainly by the stiffness of the beam. When fatigue failure of the structural system occurs, there is a slight change in the rail deflection. However, the impact of this change on the track smoothness is insignificant.

(4) The stress redistribution of the track–bridge structural system subjected to the train fatigue load has a more significant effect on the track structure layer stress than on the beam stress.

(5) As environmental factors such as temperature are not considered, and the structural system is only subjected to the train load action, the track system interlayer bond remains intact. Therefore, the calculated results of the interface cohesive zone model and spring model are basically consistent.

(6) The fatigue degradation of the CA mortar layer has a significant impact on the structural system, which directly affects structural layer stress variation with the fatigue loading cycle. The damage evolution of structural system is closer to reality when considering the CA mortar layer fatigue degradation.

6. Further Research

As the interface fatigue damage is not considered in this paper, to simulate the actual interface situation, it is necessary to carry out research on interface fatigue damage test and fatigue cohesive zone model in the future to improve the finite element model developed in this paper.

Author Contributions: Conceptualization, L.Z., L.Y., Z.S., X.P. and A.D.M.; methodology, L.Z., L.Y., Z.S., X.P. and A.D.M.; software, L.Z., L.Y., Z.S., X.P. and A.D.M.; validation, L.Z., L.Y., Z.S., X.P. and A.D.M.; formal analysis, L.Z., L.Y., Z.S., X.P. and A.D.M.; investigation, L.Z., L.Y., Z.S., X.P. and A.D.M.; resources, L.Z., L.Y., Z.S., X.P. and A.D.M.; data curation, L.Z., L.Y., Z.S., X.P. and A.D.M.; writing—original draft preparation, L.Z., L.Y., Z.S., X.P. and A.D.M.; writing—review and editing, L.Z., L.Y., Z.S., X.P. and A.D.M.; visualization, L.Z., L.Y., Z.S., X.P. and A.D.M.; supervision, L.Z. and Z.S.; project administration, L.Z. and Z.S.; funding acquisition, L.Z. and Z.S.

Funding: This research was supported by the National Natural Science Foundation of China, grant numbers 51578546, U1434204, 51820105014, 51808558; the Natural Science Foundation of Hunan Province, China, grant number 2019JJ50800; the China Energy Investment Corporation, grant number SHGF-18-50.

Acknowledgments: Special thanks go to the reviewers for their valuable suggestions. The authors also would like to thank their colleagues at Central South University for research design, etc.

Conflicts of Interest: The authors declare no conflict of interest.

References

1. Zhou, M.; Dai, G.L. Stability of longitudinally connected ballastless slab track on simply-supported beam bridges of high-speed railway. *J. China Railw. Soc.* **2015**, *37*, 60–65. (In Chinese)
2. Sun, L.; Chen, L.; Zelelew, H.H. Stress and Deflection Parametric Study of High-Speed Railway CRTS II Ballastless Slab on Elevated Bridge Foundations. *J. Transp. Eng.* **2013**, *139*, 1224–1234. [CrossRef]
3. Konings, P. A Study on the Lifetime Aspects of the Rheda 2000 Track System. Ph.D. Thesis, Delft University of Technology, Delft, The Netherlands, 2005.
4. Wang, Q.; Wei, J.; Dong, R.Z. Fatigue behavior analysis of CRTS II slab ballastless track structure. *J. Railw. Eng. Soc.* **2014**, *31*, 41–47.
5. Poveda, E.; Rena, C.Y.; Lancha, J.C.; Ruiz, G. A numerical study on the fatigue Life design of concrete slabs for railway tracks. *Eng. Struct.* **2015**, *100*, 455–467. [CrossRef]
6. Zhu, S.Y.; Cai, C.B. Fatigue damage model of concrete structure for ballastless track of high speed railway. *Sci. Sin. (Technol.)* **2014**, *44*, 714–721.

7. Chen, R.P.; Wang, Z.Z.; Jiang, H.G.; Bian, X.C. Control standard of differential settlement in high-speed railway slab based on bending fatigue strength. *J. Zhejiang Univ. (Eng. Sci.)* **2013**, *47*, 796–802.
8. Tarifa, M.; Zhang, X.; Ruiz, G.; Poveda, E. Full-scale fatigue tests of precast reinforced concrete slabs for railway tracks. *Eng. Struct.* **2015**, *100*, 610–621. [CrossRef]
9. Liu, F.S.; Zeng, Z.P.; Wu, B.; Zhang, Z.C.; Peng, K. Study of the Effect of Cement Asphalt Mortar Disease on Mechanical Properties of CRTS II Slab Ballastless Track. *Adv. Mater. Res.* **2014**, *906*, 305–310. [CrossRef]
10. Du, H.Y.; Liu, G.; Su, C.G. Fatigue Behavior of CA mortar layer in CRTS-I Ballastless Track under Train Load. *Appl. Mech. Mater.* **2013**, *405–408*, 40–44. [CrossRef]
11. Li, Y.L.; Zhao, J.Y.; Ou, Y.J.; Tan, Y.Q. Fatigue behavior of CA mortar layer. *China Sci.* **2012**, *7*, 846–848.
12. Wang, F.Z.; Liu, Z.C. Research on the Fatigue Behavior of CA Mortar Layer Used in Ballastless Slab Track of High Speed Railway. *Journal of Wuhan University of Technology* **2008**, *11*, 79–81.
13. Zhu, S.Y.; Fu, Q.; Cai, C.B.; Spanos, P.D. Damage evolution and dynamic response of cement asphalt mortar layer of slab track under vehivle dynamic load. *Sci. China Technol. Sci.* **2014**, *57*, 1883–1894. [CrossRef]
14. Zhu, S.Y.; Cai, C.B. Interface damage and its effect on vibrations of slab track under temperature and vehicle dynamic loads. *Int. J. Non-Linearmech.* **2014**, *58*, 222–232. [CrossRef]
15. Zhong, Y.L.; Gao, L.; Wang, P.; Liang, S.J. Mechanism of interfacial shear failure between CRTS II slab and CA mortar layer under temperature loading. *Eng. Mech.* **2018**, *35*, 230–238.
16. Dai, G.L.; Su, M. Mechanism of interfacial bond failure for slab ballastless track under shear loading. *J. Huazhong Univ. Sci. Technol. (Nat. Sci. Ed.)* **2016**, *44*, 16–31.
17. Feng, Y.L.; Jiang, L.Z.; Zhou, W.B. Damage destruction evolution law of high-speed railway CRTS II slab ballastless track interface under train braking and temperature load. *IOP Conf. Ser. Earth Environ. Sci.* **2018**, *189*, 062060. [CrossRef]
18. Ping, W.; Hao, X.; Rong, C. Effect of Cement Asphalt Mortar Debonding on Dynamic Properties of CRTS II Slab Ballastless Track. *Adv. Mater. Sci. Eng.* **2014**, *2014*, 193128.
19. Qi, S.X.; Ren, J.J.; Liu, X.Y. Influence of debonding on the performance of CRTSII slab track turnouts on large bridges. *Eng. Mech.* **2015**, *32*, 124–132.
20. Tian, D.M.; Deng, D.H.; Peng, J.W.; Wang, S.X.; Ai, Y.Q. Influence of temperature on interfacial bonding between Cement emulsified asphalt mortar later and concrete layer. *J. China Railw. Soc.* **2013**, *35*, 78–85.
21. Xu, Q.Y.; Zhang, Z.; Chen, X.P.; Lou, P.; Wei, Q.; Duan, J. Experimental study on fatigue life prediction model of concrete of CRTSII slab track on bridge. *J. Railw. Sci. Eng.* **2017**, *14*, 1565–1570.
22. Xu, Q.Y.; Lin, Q.T.; Feng, Z.Y.; Zhang, Z.; Lou, P.; Xiao, Z.; Duan, J. Fatigue properties of longitudinal connected slab track under Combined loads. *China Railw. Sci.* **2017**, *38*, 37–45.
23. Xu, Q.Y.; Lin, Q.T.; Feng, Z.Y.; Lou, P.; Yang, R.; Chen, W.; Zhang, Z. Theoretical study on fatigue stress spectrum of longitudinal connected slab track on bridge. *J. Southwest Jiaotong Univ.* **2018**, *53*, 906–912.
24. Yu, Z.W.; Shan, Z.; Ouyang, Z.Y.; Guo, F. A simple damage model for concrete considering irreverible mode-II microcracks. *Fatigue Fract. Eng. Mater. Struct.* **2016**, *39*, 1419–1432. [CrossRef]
25. Shan, Z. Stochastic Damage Model for Concrete and Its Application. Ph.D. Thesis, Central South University, College of Civil Engineering, Changsha, China, 2017; pp. 125–131.
26. Yu, Z.W.; Shan, Z.; Li, X. *Research on Time-Dependent Behavior of High-Speed Railway Ballastless Track-Bridge Structural System: Stochastic Viscoelastic-Damage Constitutive Model of Crts Ii Ca Mortar Layer*; Central South University: Changsha, China, 2018. (In Chinese)
27. GB 50010-2010. *Code for Design of Concrete Structures*; China Architecture & Building Press: Beijing, China, 2015; pp. 19–21.
28. The Concrete Fatigue Task Forces. *Research on Failure Reliability Checking Calculation Method of Reinforced Concrete Flexural Components*; China Construction Industry Publishing House: Beijing, China, 1994; pp. 26–27.
29. Li, P.G. Analysis of the Interface Damage of CRTS II Slab Track and Its Influences. Ph.D. Thesis, Southwest Jiaotong University, College of Civil Engineering, Chengdu, China, 2015; pp. 13–14.
30. Liu, X.Y.; Su, C.G.; Liu, D.; Xiang, F.; Gong, C.; Zhao, P.R. Research on the bond properties between slab and CA mortar layer and the parameters study of cohesive model. *J. Railw. Eng. Soc.* **2017**, *3*, 22–28.
31. TB 10015-2012. *Code for Design of Railway Continuous Welded Rail*; China Railway Publishing House: Beijing, China, 2012; pp. 6–8.

32. Gong, C. Study on Composite Specimens Mechanical Properties in CRTSII Slab Track. Master's Thesis, Southwest Jiaotong University, College of Architecture and Civil Engineering, Chengdu, China, 2017; pp. 38–41.
33. Zhu, J.S.; Zhu, X.C. Study on simplified method for the analysis of fatigue failure process of RC bridges. *Eng. Mech.* **2012**, *29*, 107–121.
34. Xiao, J.Z.; Chen, D.Y.; Zha, Q.F. Test on bend fatigue behavior of HPC simply-supported beams. *Struct. Eng.* **2006**, *22*, 72–76. (In Chinese)
35. Yu, Z.W.; Zhou, L.Y.; Zhao, L. *Research on Time-Dependent Behavior of High-Speed Railway Ballastless Track-Bridge Structural System: Cooperative Performance Test of High-Speed Railway Ballastless Track-Bridge Structural System*; Central South University: Changsha, China, 2018. (In Chinese)
36. TB10621-2014. *Design Code for High Speed Railway*; China Railway Publishing House: Beijing, China, 2014; pp. 2–3.